THE DE HAAS-VAN ALPHEN EFFECT IN CALCIUM

THE DE HAAS-VAN ALPHEN EFFECT IN CALCIUM

by

ROGER M. JENKINS B.Sc.

A Thesis

Submitted to the Faculty of Graduate Studies

in Partial Fulfilment of the Requirements

for the Degree

Master of Science

McMaster University

August, 1972

MASTER OF SCIENCE (1972)
(Physics)

MCMASTER UNIVERSITY
Hamilton, Ontario

TITLE: The de Haas-van Alphen effect in Calcium

AUTHOR: Roger M. Jenkins B.Sc. (University of Aston in Birmingham)

SUPERVISOR: Professor W.R. Datars

NUMBER OF PAGES: V, 34

SCOPE AND CONTENTS:

The de Haas-van Alphen (dHvA) effect has been studied in single crystals of calcium using the modulation method in magnetic fields up to 55 kOe. Four distinct orbits were observed with dHvA frequency minima at the [110] or [100] directions. The results do not support calculations predicting a disconnected first-band Fermi surface for calcium. The dHvA data of crystalline calcium is consistent with the topology of the two-OPW model in which the first band is connected and pockets of electrons are about the point L of the second zone.

ACKNOWLEDGEMENTS

The author wishes to thank Professor W.R. Datars for his guidance and help throughout the course of this research. I would also like to thank R. Douglas, A. Dunsworth and C. Verge for many helpful discussions. The research was supported by a grant from the National Research Council of Canada.

TABLE OF CONTENTS

LIST OF ILLUSTRATIONS

CHAPTER I

INTRODUCTION

Calcium is an alkaline earth metal of atomic number 20 with an electron configuration $1s^2$, $2s^2$, $2p^6$, $3s^2$, $3p^6$, $4s^2$ thus having two valence electrons. It has a face centred cubic structure with a = 10.5 au.[1] On exposure to air it forms a white powdery, non-conducting coating of the hydroxide. Occasionally, a black coating of unknown chemical composition forms. This is also an insulator.

The only experimental measurements of the Fermi surface of calcium have been by Berlincourt[2] and Condon and Marcus[3]. Both used the de Haas-van Alphen (dHvA) effect to obtain extremal cross-sectional areas of the Fermi surface. Berlincourt, using a pulsed-field technique, found only one frequency of $(1.7 \pm 0.15) \times 10^7$g. From the temperature dependence of the dHvA signal he obtained an effective mass of $0.61 m_o \pm 10\%$.

Condon and Marcus, using a torsion method and a maximum field of 33 kOe, measured three dHvA frequencies. However their assignment of crystal orientation to their data appears incorrect, since their results do not have the expected symmetry of a cubic structure. Also, they found their samples were polycrystaline; this made their results inconclusive when trying to fit them to a Fermi surface model.

Following these experiments there have been a series of theoretical calculations of the Fermi surface of calcium, with widely differing results. The main difference between the various calculations is whether the hole surface consists of several separate pieces, and if so, where they are situated in the Brillouin zone; or if it is a connected hole surface.

The purpose of this work was to again use the dHvA effect in calcium, using a superconducting magnet and computer analysis of the results, to clarify the experimental measurements of the Fermi surface and to see which theoretical model has the best agreement with experiment.

CHAPTER II

THEORY

1. Fermi Surface

Calcium, with a valence of two, is a compensated metal with an equal number of electrons and holes. Its Fermi surface consists of a hole surface in the first Brillouin zone and an electron surface in the second zone.

In the single-OPW model, where the ionic potential is assumed uniform throughout the crystal, the Fermi surface is obtained by the method due to Harrison[4], where spheres of radius k_f are constructed around the reciprocal lattice points. The resulting Fermi surface is shown in Fig. 1. The hole surface is multi-connected, while the electron surface consists of four lenses each centred at L in the Brillouin zone. Although this model involves the rather drastic approximation of neglecting the ionic potential, it often gives a good first approximation to the real Fermi surface in simple metals. The explanation of this comes from pseudo-potential theory which shows that the effective potential is much smaller than the ionic potential.

The major inaccuracies of the single-OPW Fermi surface occur where the surface is close to, or intersects a Bragg reflection plane. In these regions multiple OPW techniques can be used to give more accurate results. From the single-OPW model one sees these modifications should appear near the [200] and [111] faces of calcium. Using Harrison's value of 0.039 Ry and 0.003 Ry respectively

Figure 1

The single-OPW Fermi Surface.

a) The first zone hole surface.

b) The second zone electron surface.

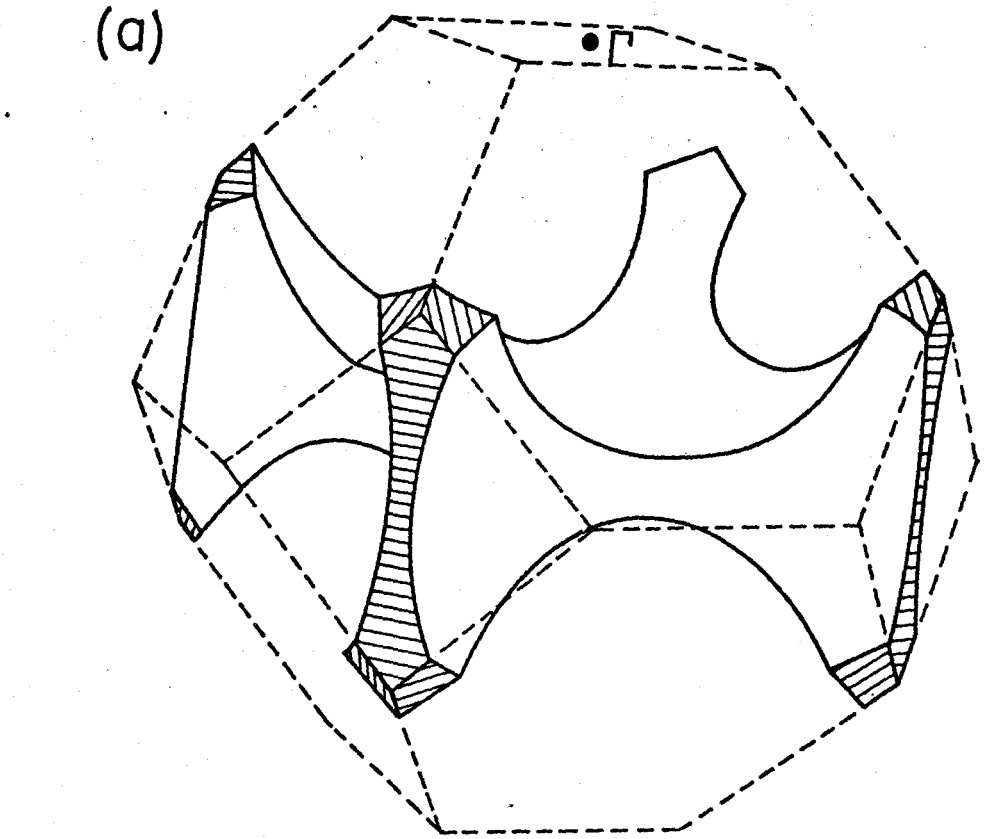
(a)
Γ

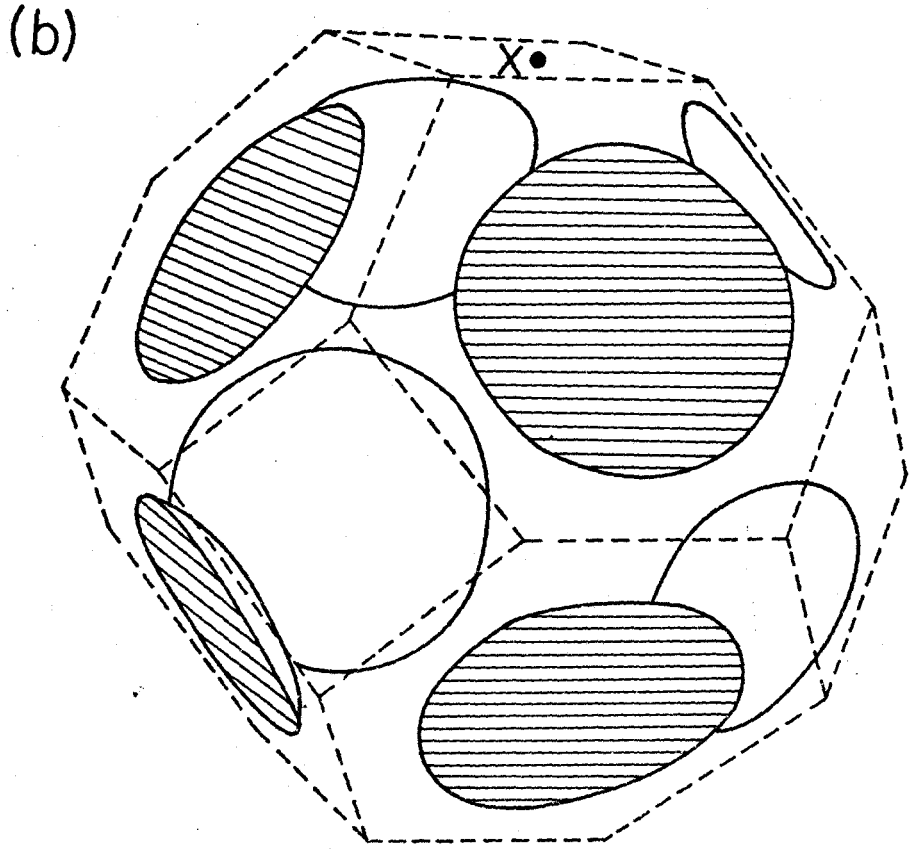
(b)
X

for the effective potential, a two-OPW calculation was carried out. The resulting Fermi surface is shown in Fig. 2. The hole surface in the [100] direction is open in the centre, although the surface remains connected by arms. The effect of the [111] faces on the electron pieces was found to be negligble in the two-OPW calculation.

Charterjee and Chakraborti[5], using a multiple-OPW method and their own calculated values of effective potential, obtained a dismembered hole surface with pockets of holes around the points K and U in first zone and the electron surface consisting of four lenses centred at L. Later[6], they used a quantum defect method and again obtained a disconnected hole surface, but with pockets of holes at W in the zone. The same electron surface was obtained.

Vasvári[7] used the full non-local pseudo-potential and obtained a Fermi surface that consists of pockets of holes around the point W, with four lenses centred at L for the electron surface. However, this result is strongly dependent on the choice of 0.33 Ry for the Fermi energy, a smaller value of 0.32 Ry results in a hole surface to that shown in Fig. 2.

In 1971 Altmann et al.[8] calculated the band structure of calcium by a celluler method using a Slater type potential. With a Fermi energy of 0.31 Ry, they obtained a connected hole surface of similar shape to that of Fig. 2. Driesen and Pyenson[9] used a first principles, non-relativistic

Figure 2

The two-OPW Fermi Surface.

a) The first zone hole surface.

b) The second zone electron surface.

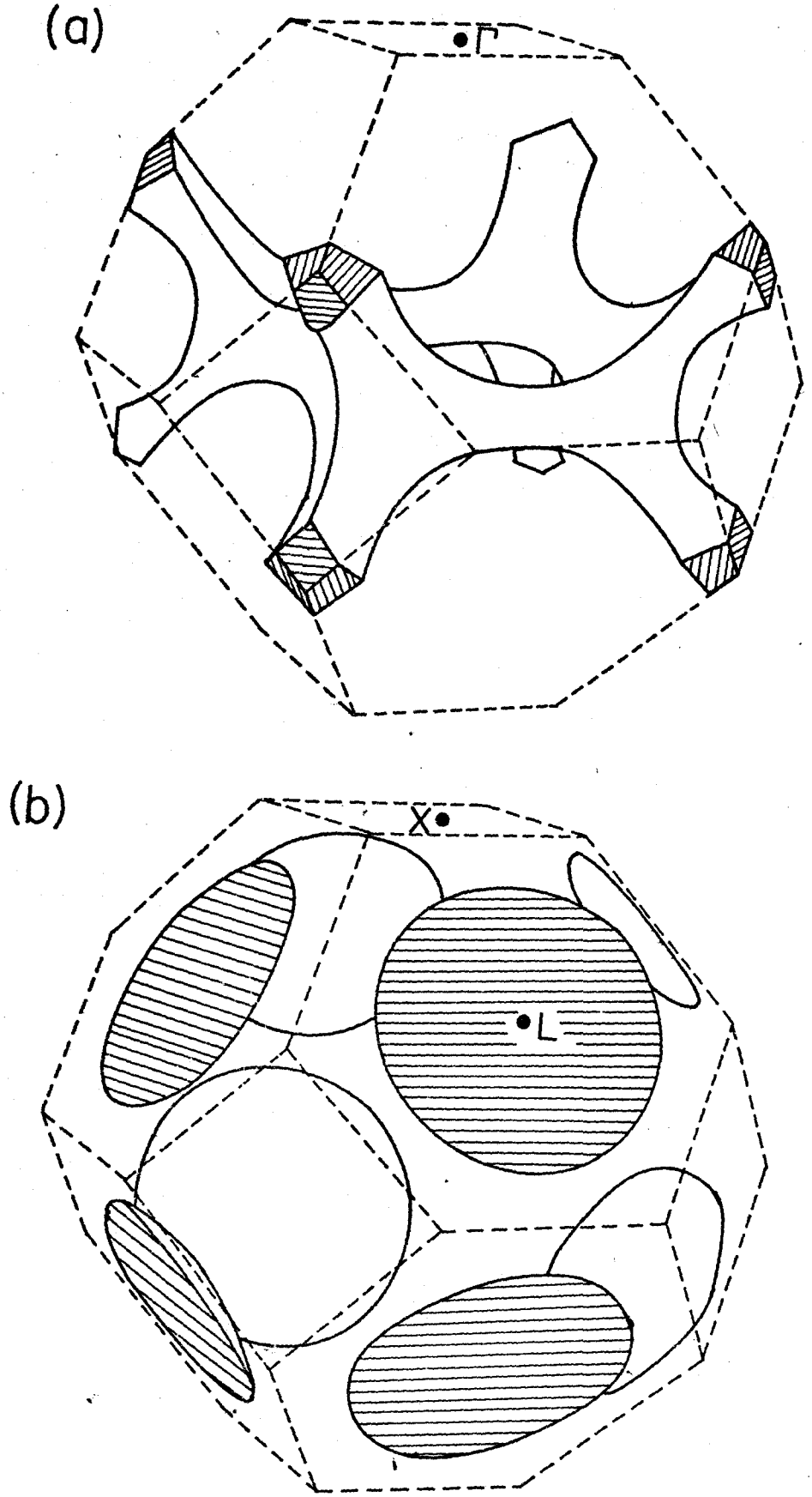
(a)
Γ
(b)
X
L

Green's function method to compute self-consistent energy bands of calcium. They calculated the Fermi energy to be 0.2918 Ry and obtained first-zone pockets of holes around the point W. Their second zone surface consists of electron lenses centred at L. They concluded that their results are very similar to those of Vasvári.

2. de Haas-van Alphen Effect

This effect is one of the main methods of measuring the Fermi surface of metals, and is an oscillatory component of the magnetic susceptibility of a crystal as a function of magnetic field. Good quality crystals at very low temperatures in fairly high magnetic fields are needed to observe the effect.

In a constant magnetic field, the allowed energy states of the conduction electrons coalesce into a set of discrete energy levels called Landau levels, because of flux quantization. Up to the Fermi energy the Landau levels are occupied but above this energy they are empty. As the magnetic field increases the Landau levels expand, and as a particular level passes through the Fermi surface it becomes de-populated and the total electronic free energy is reduced. As another level rises towards the Fermi surface the energy increases until it passes through the surface and then the free energy is again reduced. Thus, as the magnetic field changes there is a periodic emptying of Landau levels resulting in a periodic change in the free

energy of the conduction electrons, with a period determined by the interval between coincidences of a quantised orbit with the Fermi level. This energy change is observed in several physical properties of metals; the change in magnetic susceptibility is one of the most pronounced and easiest to observe experimentally.

The full mathematical treatment of the effect has been rigorously calculated by Lifshitz and Kosevich[10], and by Gold[11]. The final result is that the oscillatory part of the magnetization $\tilde{M}$ is given by

$$\tilde{M} = \frac{-e\hbar}{4\pi^4 m_c} \left(\frac{2\pi eH}{\hbar}\right)^{1/2} \left|\frac{\partial A_o}{\partial k_H}\right|^{-1/2} \left\{\hat{H} - \frac{1}{F}\frac{\partial F}{\partial \theta}\hat{\theta} - \frac{1}{F\sin\theta}\frac{\partial F}{\partial \phi}\hat{\phi}\right\}$$

$$\times \sum_{r=1}^{\infty} \frac{X_r}{\sinh X_r} \frac{K_r}{r^{3/2}} \sin\left(2\pi r\left(\frac{F}{H} - \gamma\right) \pm \frac{\pi}{4}\right) .$$

$\{\hat{H}, \hat{\theta}$ and $\hat{\phi}\}$ is a set of orthogonal unit vectors when the field is expressed in spherical polar co-ordinates.

m_c is the cyclotron mass.

$\left|\frac{\partial A_o}{\partial k_H}\right|^{-1/2}$ is a factor related to the curvature of the Fermi surface in the region of the orbit.

r is an index indicating harmonic number.

$\frac{X_r}{\sinh X_r}$ is the term containing the temperature dependence of the signal where $X_r = \frac{2\pi^2 r\, m_c k_o T}{e\hbar H}$.

K_r includes the effect of scattering of the electrons and is expressed by $K_r = \exp\left(\frac{-2\pi r m_c k_o T_D}{e\hbar H}\right)$

where T_D is the Dingle temperature.

A_o is an extremal area of the Fermi surface in the plane normal to the magnetic field direction.

F is the dHvA frequency equal to $\frac{\hbar A_o}{2\pi e}$.

Thus the frequency of a dHvA oscillation in 1/H is directly proportional to an extremal cross-sectional area of the Fermi surface normal to the magnetic field direction. In this way measurements of the Fermi surface are made. By measuring the variation of the dHvA signal amplitude with temperature at a fixed value of magnetic field one can calculate the cyclotron mass of the electrons; similarly, by measuring the dependence of the dHvA signal amplitude with the magnetic field strength at constant temperature one can calculate the Dingle temperature.

CHAPTER III

EXPERIMENTAL METHOD

The calcium samples, obtained from J. McCreary[12], were grown by a fractional distillation process. They were typically 2 cm long and up to 1 cm in diameter with numerous growth faces. Since calcium reacts rapidly in air to form a surface layer of oxide or hydroxide, which eventually transforms a sample into a white powder, samples were handled with minimum exposure to air. The surface layer made X-ray analysis very difficult. However, some results were obtained using Laue back reflection and precession techniques which indicated that the samples were not single crystals, but rather a large number of crystals joined together. A solution of one part hydrochloric acid and three parts methanol removed the surface layer and etched the crystals. Attempts to encapsulate the crystals in wax after etching were unsuccessful because the coating did not completely stop the oxidation process. To obtain a possible single crystal of suitable size for experimental use, a small part of the crystal, typically 3 × 2 × 2 mms., was cut from the larger piece by the acid-saw method. Cotton thread was used to transport the cutting solution of hydrochloric acid and methanol across the crystal. This technique was found to work well and produce a narrow, strain free cut. The sample was then glued into a Kel-F holder with a small amount of Glyptal cement.

Because of the difficulties encountered using X-rays to examine the crystals, instead of the conventional method of X-ray orientation of the sample prior to mounting, or using the morphology of the crystal as used by Condon and Marcus, crystals were mounted with no preconceived concept of orientation and the determination of orientation was attempted from the symmetry of the dHvA data. Out of ten samples examined four appeared to be predominantly single crystals and it was possible to orient three. The sample, glued in the holder, was inserted into a modulation and pick-up coil assembly, with a turning mechanism allowing the crystal to be rotated through 360°.

The modulation method[13] was used to detect the dHvA signals. Since the magnetization of the crystal is a non-linear function of the magnetic field, harmonics of the modulation frequency are generated inductively in the pick-up coil placed around the sample. The dHvA signal at any desired harmonic frequency is selectively amplified and synchronously detected. A schematic diagram of the apparatus is shown in Fig. 3. The magnetic field was provided by a Westinghouse 55 kOe superconducting magnet that could be swept in 1/H. A modulation frequency of 517 Hz was used with a typical modulation field of 80 Oe. The pick-up coils were impedence matched to a twin-T filter which was used to remove the fundamental frequency. A PAR HR-8 lock-in amplifier was used to detect the second harmonic signal. A data acquisition system was used to record digitally

Figure 3

Block diagram of apparatus

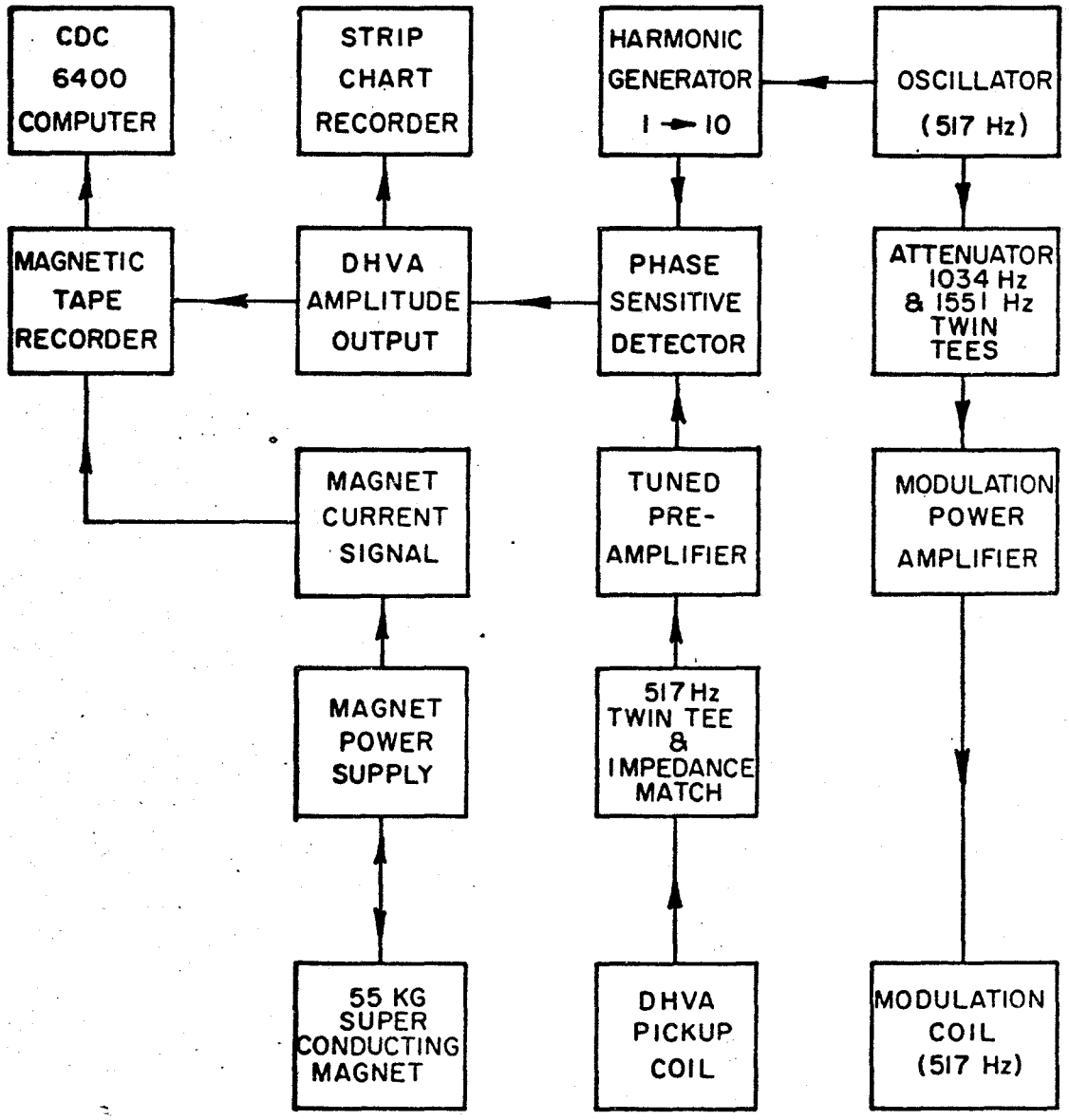
CDC 6400 COMPUTER
STRIP CHART RECORDER
HARMONIC GENERATOR 1 → 10
OSCILLATOR (517 Hz)
MAGNETIC TAPE RECORDER
DHVA AMPLITUDE OUTPUT
PHASE SENSITIVE DETECTOR
ATTENUATOR 1034 Hz & 1551 Hz TWIN TEES
MAGNET CURRENT SIGNAL
TUNED PRE-AMPLIFIER
MODULATION POWER AMPLIFIER
MAGNET POWER SUPPLY
517 Hz TWIN TEE & IMPEDANCE MATCH
55 KG SUPER CONDUCTING MAGNET
DHVA PICKUP COIL
MODULATION COIL (517 Hz)

the dHvA signal together with magnetic field values on magnetic tape for subsequent computer analysis. Typically ten pairs of field and signal readings were recorded per dHvA oscillation, over approximately 500 oscillations. The field was swept from 30 to 50 kOe which resulted in an error in the measured frequency of ±4 Tesla. A fast Fournier transform programme was used to determine the dHvA frequencies at each magnetic field direction. All measurements, except the temperature dependence of the signal, were done at 1.2°K with the sample immersed in liquid helium kept at a low vapour pressure by pumping. For the temperature dependence of the signal, a Texas Instrument precision pressure gauge was used to measure the pressure of the helium gas above the sample. The signal amplitude was measured at a fixed magnetic field value in temperature range 1.2 to 3°K at approximately 0.2°K intervals.

CHAPTER IV

RESULTS

The results obtained from sample 1 are shown in Fig. 4. Discussion of the assignment of the crystallographic directions is given in the next section. Three distinct dHvA frequency ranges are clearly seen. The low-frequency range consists of three branches A_1, A_2 and A_3 each with an angular range of approximately 60° and a minimum frequency of 340 Tesla. A fourth branch, A_4, extending over 40° has a minimum frequency of 420 Tesla. The mid-frequency range extends from 1270 Tesla to 1400 Tesla. Again there are four branches, although B_2 is split and has a much weaker angular dependence than the other three. Finally there are four high-frequency branches, each with a minimum frequency of 1720 Tesla. Two branches C_1 and C_2 are not continuous and can be followed in frequency up to about 2,500 Tesla. The dHvA signal decreases in amplitude as the field direction moves away from the minimum frequency orientation. The other two branches are continuous through 180°, C_3 having a maximum frequency of 2085 Tesla, and C_4 a maximum frequency of 2,310 Tesla. Second and higher harmonics of most of the dHvA frequencies were detected but these are omitted from Fig. 4. Sums of $(B_4 + C_1)$ and $(B_4 + C_2)$ were also observed. Several other frequency points, especially in the 1720 to 1800 Tesla range, were detected which did not fall on any well defined line, and were of smaller amplitude

Figure 4

dHvA frequency spectrum of sample 1.

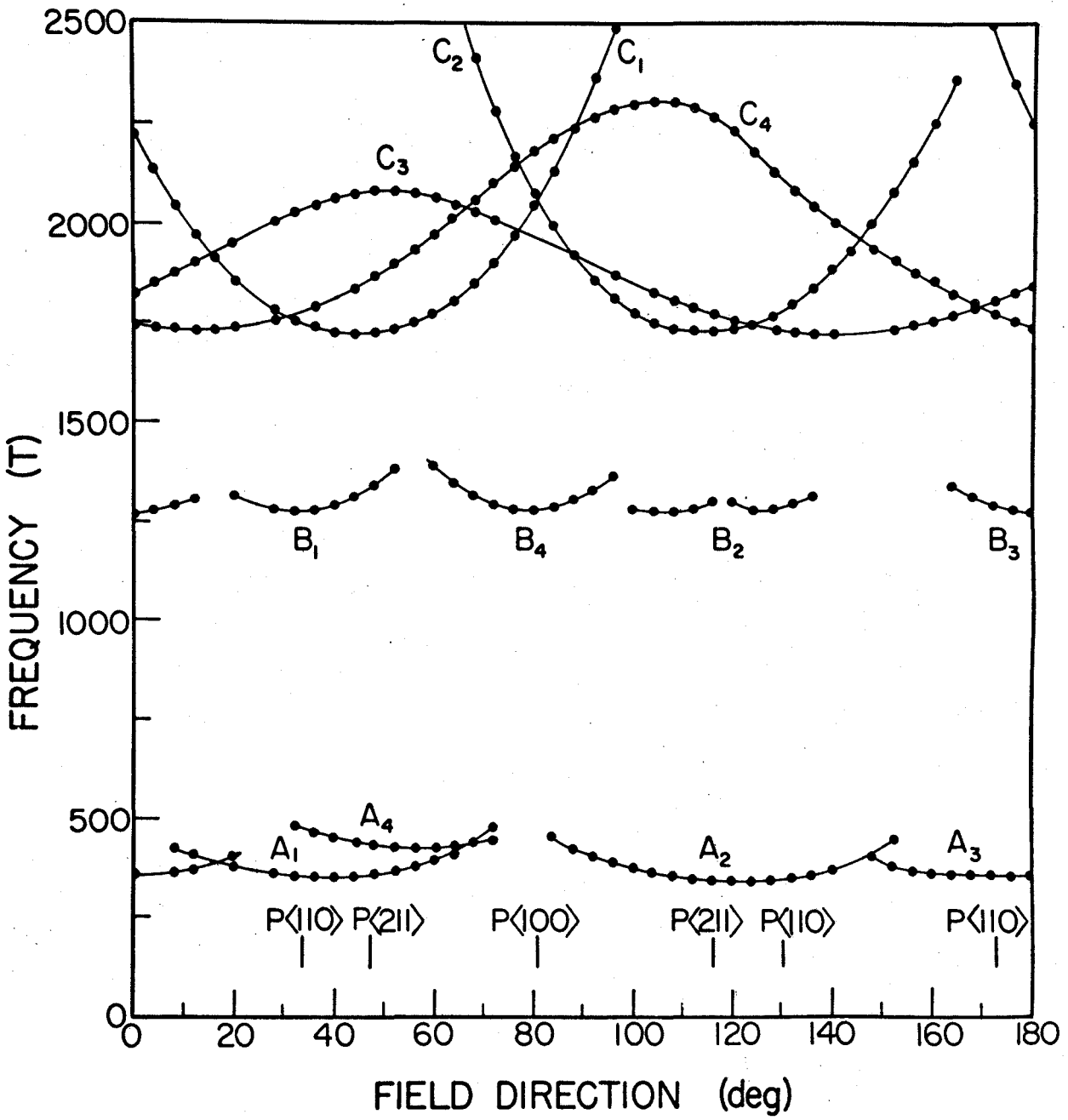
2500
2000
1500
1000
500
0
FREQUENCY (T)
C2
C1
C4
C3
B1
B4
B2
B3
A4
A1
A2
A3
P⟨110⟩ P⟨211⟩
P⟨100⟩
P⟨211⟩ P⟨110⟩
P⟨110⟩
0 20 40 60 80 100 120 140 160 180
FIELD DIRECTION (deg)

than those shown in Fig. 4. These points are assigned to smaller crystals present in the sample.

The results obtained from sample 2 are shown in Fig. 5. Again three frequency regions are seen. There are three low-frequency branches each with minimum frequency of 325 Tesla, the minima each being separated by 60°. The extent of each branch is approximately 70° so that this low-frequency is observed in all field directions. In the mid-frequency range there are four branches, although B_3 was not a strong signal and has a smaller angular dependence than the other three. The high frequency branches are interesting. C_1 is isotropic with a frequency of 1724 Tesla, while the other three branches have minimum frequencies of 1722 Tesla and show three-fold symmetry. The cross-over frequency of these three branches is 1950±20 Tesla. Again there was evidence of other smaller crystals in the sample, giving rise to weaker, random signals not shown in Fig. 5.

Fig. 6 shows the results obtained from sample 3. This sample was much smaller than the others used, being approximately 2 mms by 1 mm by 1 mm; the results indicated this was a single crystal. There are three main branches in the low-frequency region, each with a minimum frequency of 345 Tesla, while two branches A_4 and A_5 from weaker signals are present from 40° to 70° and 130° to 175° respectively. The minimum frequency of these two branches is 450 Tesla. No low-frequency signal was observed between

Figure 5

dHvA frequency spectrum of sample 2.

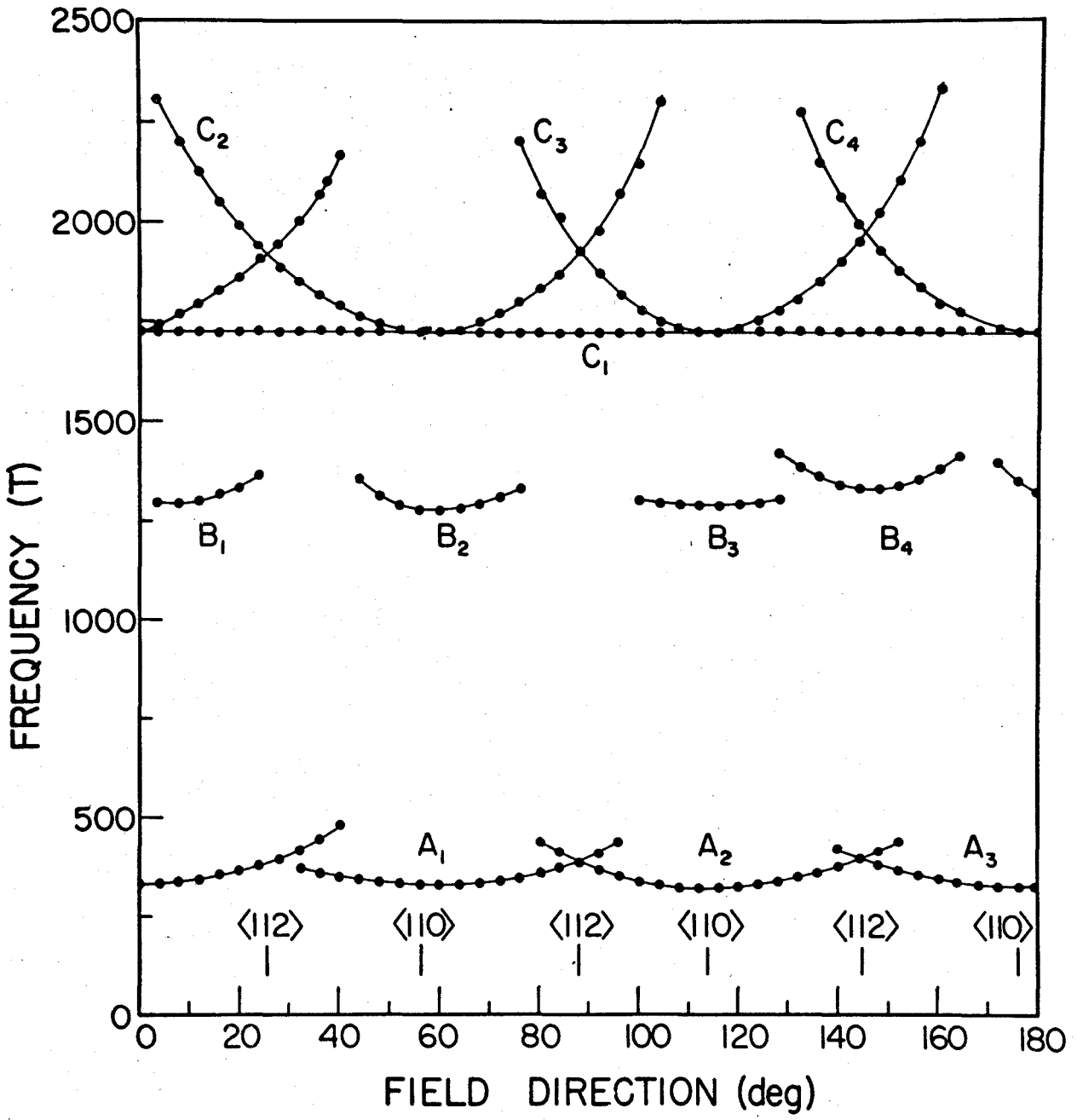
2500
2000
1500
1000
500
0
FREQUENCY (T)
C2
C3
C4
C1
B1
B2
B3
B4
A1
A2
A3
⟨112⟩
⟨110⟩
⟨112⟩
⟨110⟩
⟨112⟩
⟨110⟩
0
20
40
60
80
100
120
140
160
180
FIELD DIRECTION (deg)

Figure 6

dHvA frequency spectrum of sampel 3.

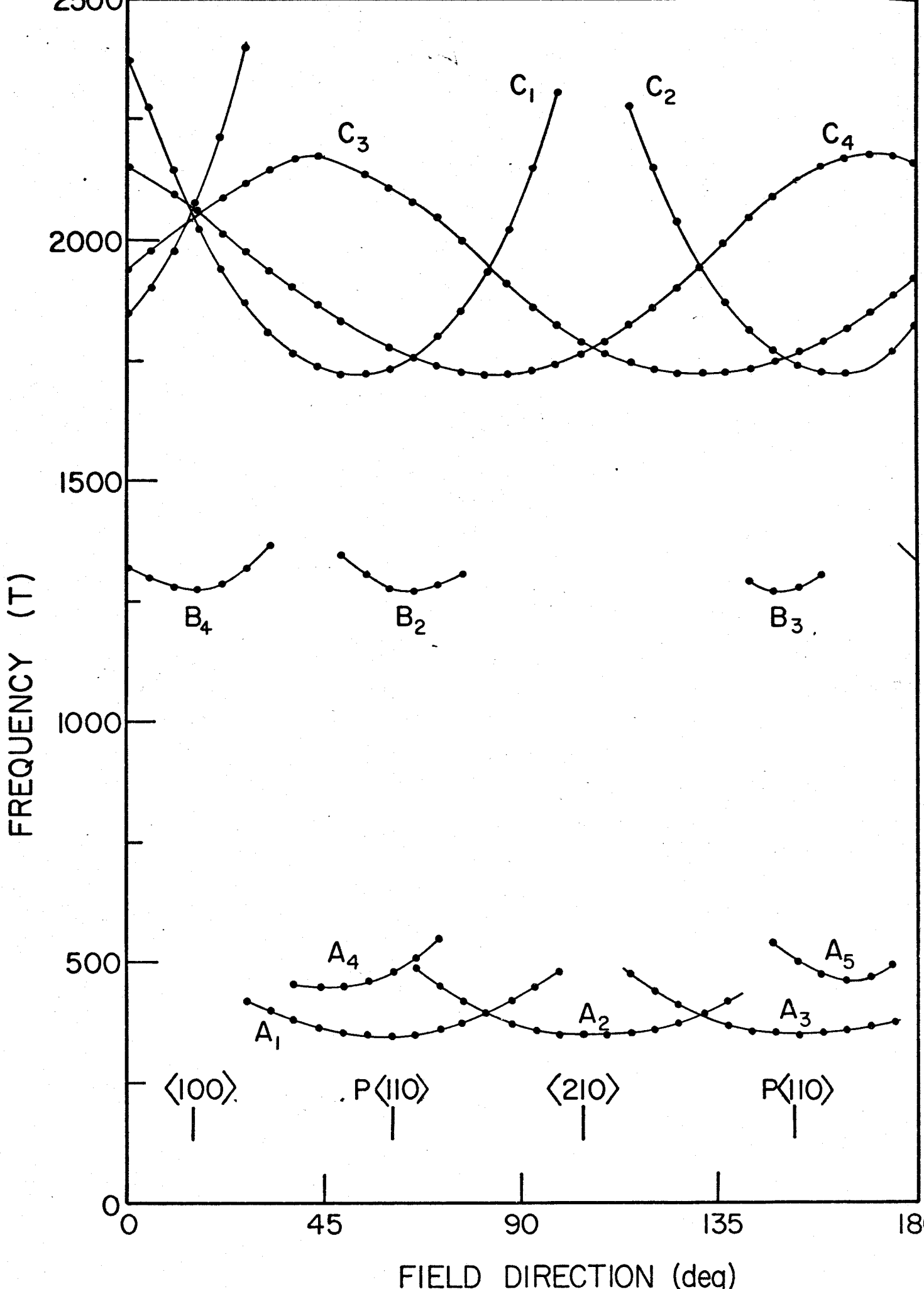
2500
2000
1500
1000
500
0
FREQUENCY (T)
C1
C2
C3
C4
B4
B2
B3
A4
A5
A1
A2
A3
⟨100⟩
P⟨110⟩
⟨210⟩
P⟨110⟩
0
45
90
135
180
FIELD DIRECTION (deg)

5° and 25°. In the mid-frequency range a strong branch B_4 was found between 0° and 33°, with a minimum frequency of 1278 Tesla. Two, much weaker, branches B_2 and B_3 were also present in this mid-frequency range; they both have a minimum frequency of 1270 Tesla. In the high-frequency range there are two open branches C_1 and C_2, again as the frequency increases the signal was found to decrease in strength, preventing these branches from being followed to higher frequencies. The other two branches can be followed through the 180° rotation. Both have the same maximum frequency of 2180 Tesla, while all four have the same minimum frequency of 1720 Tesla. At 15° all four branches have the same frequency of 2060 Tesla, this is also the orientation of the minimum of the strong branch B_4.

The cyclotron mass at the minimum of the branch B_4 was determined from the temperature dependence of the amplitude of the signal; this gave a value of $0.52 \pm 5\%\ m_o$. Using this value of the mass, the Dingle temperature was calculated from the field dependence of the signal. A value of 1.1°K±10% was obtained.

Finally the results from sample 4 are shown in Fig. 7. Again three frequency ranges were observed. The cyclotron mass at the minimum of one of the high frequency branches was measured and found to be $0.60\ m_o \pm 5\%$.

Figure 7

dHvA frequency spectrum of sample 4.

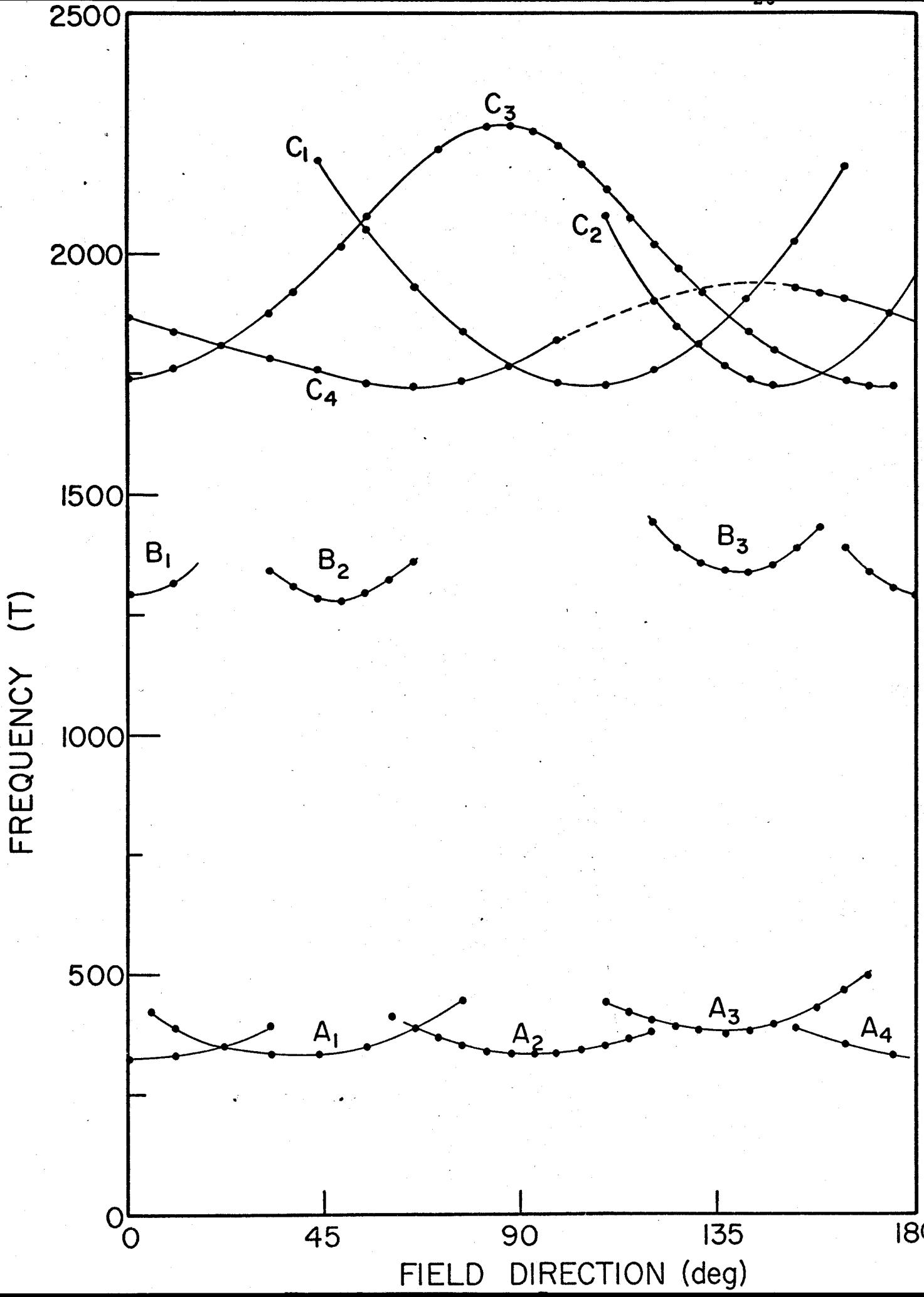
2500
2000
1500
1000
500
0
FREQUENCY (T)
C3
C1
C2
C4
B1
B2
B3
A1
A2
A3
A4
0
45
90
135
180
FIELD DIRECTION (deg)

CHAPTER V

DISCUSSION OF RESULTS

I shall use the two-OPW Fermi surface model to interpret the results, and at the end of this section compare the fit of this model with the results, with the various other Fermi surfaces proposed for calcium.

In the two-OPW Fermi surface the principle orbits likely to be detected experimentally are, following Harrison[14]

- α An orbit around the intersection of the four first zone arms, seen when the magnetic field is along a [100] crystal axis. It has a predicted minimum frequency of 1316 Tesla.
- β An orbit around the second band lens. The minimum area is seen with the magnetic field along a [110] direction, and has a frequency of 2000 Tesla.
- δ Another orbit around the junction of the four first band arms, but with the field in a [110] direction. The predicted minimum frequency is 1410T.
- γ The minimum section of a first band arm, corresponding to orbits with the field in a [110] direction, and a predicted minimum frequency of 233 Tesla.
- ζ A nearly circular orbit around the inside of the four arms. It should be seen with the field in a [100] direction, while its predicted minimum frequency is 3,330 Tesla.

η An approximately square orbit around the outside of the four arms, its predicted minimum frequency is 11,760 Tesla with the magnetic field in the [100] direction.

In all four samples four high frequency branches were observed, each branch having a minimum frequency of 1720 Tesla. In all cases these branches were either continuous throughout the 180° rotation, or gradually decreased in strength as the frequency increased, until the signal was undetectable. These results indicate that these frequencies come from four separate closed pieces of the Fermi surface. Thus it is concluded these branches originate from the four lenses of the electron surface in the second Brillouin zone; the 2-OPW calculation predicts a minimum frequency of 2,000 Tesla which is in reasonable agreement with the experimental value.

The sample orientation was found by using the symmetry of the data, together with a computer simulation of the electron Fermi surface. The computer model consisted of four ellipsoids of revolution about the [111] direction, centred at L in the Brillouin zone. The dimensions of the lenses were obtained from the experimentally observed minimum frequency of 1720 Tesla and a maximum frequency of 12,000 Tesla obtained from the two-OPW calculation.

Fig. 8 shows the high-frequency branches together with the computed high-frequency branches for an orientation

Figure 8

Comparison of experimental and theoretical high-frequency branches of sample 1. The dots are the experimental points while the continuous line is the computer fit.

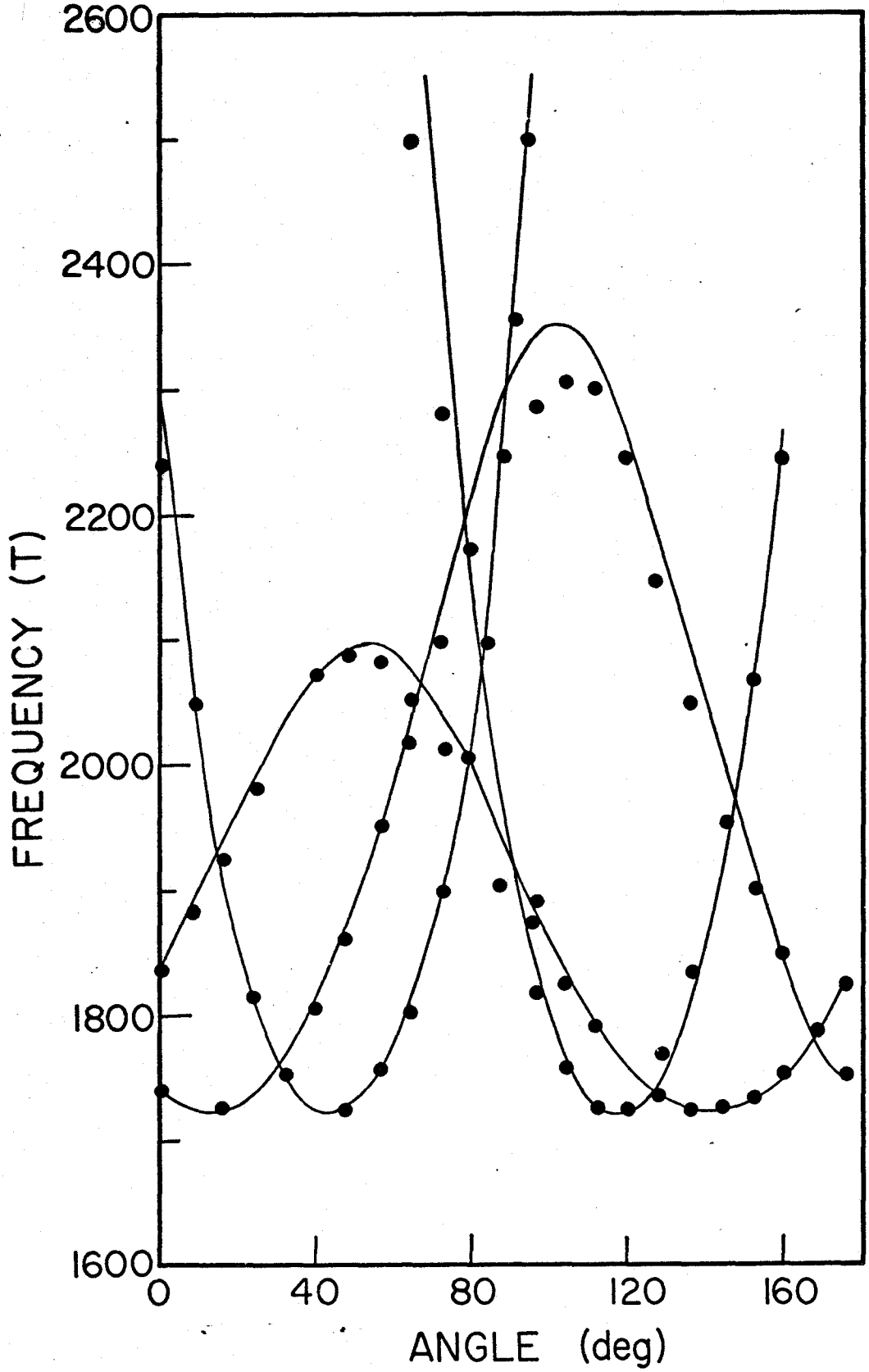
2600
2400
2200
2000
1800
1600
FREQUENCY (T)
0
40
80
120
160
ANGLE (deg)

that is 20° from the [110] direction in a [001] plane and 5° from the [010] direction in a [100] plane. It is seen there is good agreement, and by calculating the frequency spectrum for planes close to the one plotted, it appears that the plane of rotation of the sample is that specified above, to within ±2° in each direction. Using this, the orientations are marked on Fig. 4 where the letter P indicates a principle crystal direction projected onto the plane of rotation.

The three low-frequency branches A_1, A_2 and A_3 all have their lowest frequencies on projected [110] directions. These correspond to orbits of type γ around one arm of the hole surface. The fourth low frequency branch is also from an orbit of type γ, the higher frequency indicating that the orientation for its minimum area to be observed is well off the axis of rotation. No low frequency dHvA signal occurs in the vicinity of the projection of the [100] direction on the plane of rotation.

The branch B_4 has its minimum frequency of 1280 Tesla on the projection of the [100] direction and is assigned to be from an orbit of type α. The other mid-frequency branches B_1, B_2 and B_3 are all close to projections of [110] directions and are due to orbits of type δ.

The two open-ended high frequency branches C_1 and C_2 both have their minimum frequency in P[211] directions and are degenerate in the P[100] direction as expected from two of the electron lenses.

The results of sample 2 shown in Fig. 5 have three-fold symmetry which immediately indicates that the plane of rotation is a [111] plane. With this orientation one of the lenses has its smallest area perpendicular to the magnetic field direction for all directions in this plane; this results in the brach C_1 which has a constant frequency of 1724±4 Tesla. The other three branches C_2, C_3 and C_4 have their minima in [110] directions and cross each other in the [112] direction.

The mid-frequency branches B_1, B_2 and B_3 are due to orbits of type δ. The origin of B_4 is not obvious, but it is probably from an orbit of type α, since the plane of rotation is about 40° from the [100] direction at the orientation of B_4.

The three low frequency branches, due to orbits of type γ, have their minima in the [110] direction and are degenerate in the [211] directions.

Fig. 9 shows the high frequency branches obtained from sample 3, together with the computer simulation of a [210] axis of rotation. There is good agreement between the two, the presence of a mirror plane in the data, and the four-fold degeneracy of the high frequency branches at 15° verifies that the axis of rotation of the crystal is a [210] direction. The four high-frequency branches are degenerate with a frequency of 2060 Tesla with the field in the [100] direction. The minimum of branch B_4 is also

Figure 9

Comparison of experimental and theoretical high-frequency branches of sample 3. The dots are the experimental points while the continuous line is the computer fit.

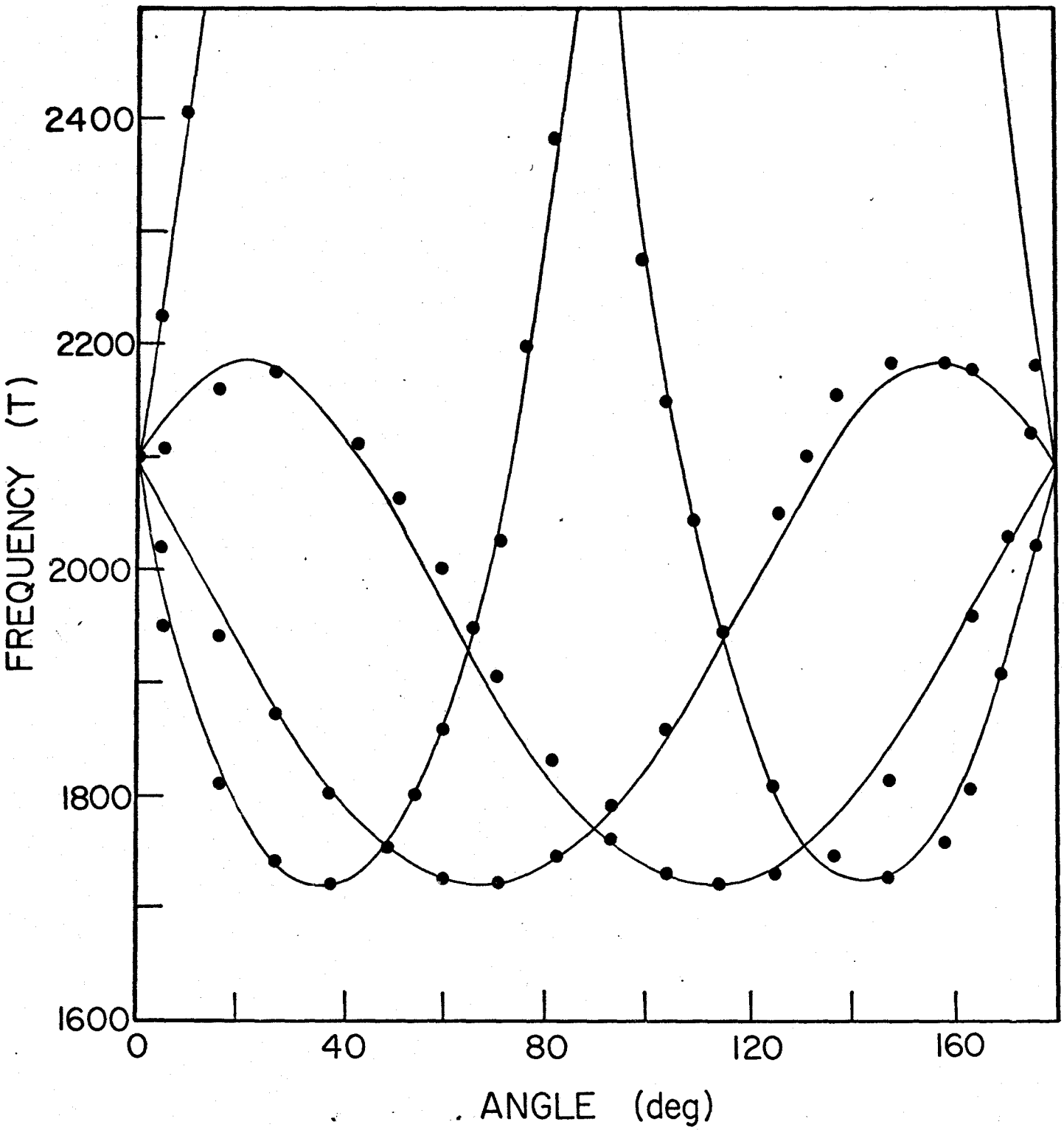
2400
2200
2000
1800
1600
FREQUENCY (T)
0
40
80
120
160
ANGLE (deg)

in this orientation, thus B_4 is due to an orbit of type α. The weaker branches B_2 and B_3 are on projected [110] directions and are due to orbits of type δ. The low-frequency branches A_1, A_2 and A_3 also have their minima in the vicinity of the projection of [110] directions onto the plane of rotation and are due to orbits of type γ. Branches A_4 and A_5 are also due to the same type or orbit, but the orientation for their minimum area to be observed is well off the axis of rotation, hence their higher frequencies. Again, no low frequency signals were observed near the [100] direction. An attempt was made to detect higher frequencies in the region around the [100] direction, but with no success.

In the case of sample 4, although the same types of frequency branches were present, the axis of rotation appears to be well away from any major symmetry direction of the crystal and no satisfactory orientation could be found.

Thus using a 2-OPW model of the Fermi surface I have been able to explain the origin of all the frequency branches measured experimentally. Four distinct orbits have been detected as summarized in table 1.

I was unable to measure the masses corresponding to orbits δ or γ because neither frequency dominated the dHvA signal in any orientation.

Thus the simple 2-OPW model is in good agreement

with the experimental results for all the frequencies measured. However, in the 2-OPW model two higher frequencies should exist in the [100] direction, but neither of these were experimentally observed. When the nature of these orbits is considered this is not really surprising. Orbit ζ, the nearly circular orbit around the inside of the four arms should have a frequency of approximately 3,000 Tesla, but with a very limited angular range. The curvature factor $\left|\frac{\partial A_H}{\partial k_H}\right|^{-1/2}$ in the expression for the dHvA amplitude will be dominant for this orbit, making the orbit difficult to detect experimentally.

The other orbit η, around the outside of the four arms has a predicted frequency of about 12,000 Tesla. The sample was probably not pure enough for this orbit to be observed.

In no case was there any indication of any of the low-frequency branches being connected to each other, similarly the mid-frequency branches were completely isolated from each other. In both frequency ranges, there was often a sharp cut-off of the dHvA signal as the crystal was rotated through a few degrees. Thus it appears extremely unlikely that these frequency branches originate from closed pieces of the Fermi surface. Very few of the theoretical papers quote expected extremal areas; the results of Vasvari, whose model seems typical of the unconnected hole surface type, do

TABLE 1

Orbit	Field Direction	Expt. Frequency (T)	2-OPW Frequency (T)	m_c/m_o
α	[100]	1275	1310	0.52
β	[110]	1720	2000	0.60
δ	[110]	1270	1408	
γ	[110]	325	233	

not agree with our measured frequencies.

In his model there are three extremal areas which give dHvA frequencies of 2210, 2941 and 1450 Tesla. The first frequency is from the electron surface, while the other two are from the hole surface. These values do not agree with the ones found, and in his model there is no orbit corresponding to the low frequency branch of 325 Tesla.

Altmann, in his third Fermi surface model for calcium, obtained a first band surface similar to the 2-OPW model. His minimum frequency for orbits of type γ is 263 Tesla compared with 325 Tesla obtained experimentally, and for the orbit β 1470 Tesla compared with the experimental value of 1720 Tesla. He has ignored the orbits α and δ although they exist in his model, and has calculated frequencies of some rather obscure orbits on his Fermi surface, none of which match with the present data.

Experiments were also done to look for open orbits in calcium (Appendix 1). The results indicated that there are open orbits, which is further evidence that calcium has a connected Fermi surface.

CONCLUSIONS

Orientations of single crystals of calcium have been determined using symmetry of dHvA data. Four distinct orbits have been detected with minimum areas in [110] or [100] directions. The dHvA data is consistent with the topology of a two-OPW model of the Fermi surface in which the first-band hole surface is connected and there are pockets of electrons about L in the second zone. The measured frequencies agree to within 20% of those predicted by this simple model, using Harrison's OPW form factors.

APPENDIX 1

With a multiply connected Fermi surface there is the possibility that for some magnetic field directions the path of an electron will not be a closed orbit. It is easiest to visualize the mechanism for this in the repeated zone scheme. The electron passes into an adjacent zone where the Fermi surface contacts a zone boundary. An example of such an "open orbit" would be the [100] direction in the single-OPW model of calcium.

The existence of an open orbit has a significant effect on the conductivity tensor σ.[15] In the high field limit, the transverse components of σ have a $1/H$ dependence for closed orbits, but for open orbits they are independent of H.

This results[16] in the induced torque saturating in the high field limit for closed orbits, but in an open orbit direction, the induced torque increases as H^2 without limit.

The induced torque magnetometer used consists of an electrically nulling galvanometer as described by Vanderkooy and Datars[17]. The sample was mounted in a Kel-F holder and suspended from the moving coil of the galvanometer by a quartz rod. The induced torque was generated by rotating a constant magnetic field about a vertical axis through the sample. The magnet used was a twelve inch electromagnet which provided a maximum field of 22 kOe. The sample could be rotated about a fixed horizontal axis while still in the

apparatus, allowing solid angle data to be taken during one experiment. Several samples, mounted with random orientation were used. In one of these open orbit peaks were observed, although they were small because the field required to produce saturation was only slightly lower than the maximum field available. Three separate sets of open orbits were observed, but it is thought they did not all originate from the same crystal. Because of this, the direction of the open orbit could not be determined, although from the 2-OPW model it appears that an open orbit in the [110] direction is possible.

BIBLIOGRAPHY

1. H. Melsert, T.J. Tiedema and W. Burgers. Acta Cryst. (1956) 9, 525.
2. T. Berlincourt. Proceedings of the Seventh International Conference on Low-Temperature Physics.
3. J. Condon and J. Marcus. Phys. Rev. 134 A446 (1964).
4. W. Harrison. Solid State Theory p. 110.
5. S. Chatterjee and D. Chakraborti. J. Phys. F. Metal Phys. 1, 638, 1971.
7. B. Vasvári. Rev. Mod. Phys. 40, 776, 1968.
8. S. Altmann, A. Harford and R. Blake. J. Phys. F. Metal Physics 1, 791, 1971.
9. J. Dreisen and L. Pyenson. Phys. Rev. B. 2, 4852, 1970.
10. I. Lifshitz and A. Kosevich. Soviet Phys. JETP 2, 636 (1956).
11. A. Gold. Solid State Physics. Vol. 1. p. 39.
12. W. McCreary. J. Metals, 10, 615 (1958).
13. R. Stark and L. Windmiller. Cryogenics 8, 272 (1968).
14. W. Harrison. Phys. Rev. 131, 2442 (1963).
15. A. Pippard. The Dynamics of Conduction Electrons, p. 81.
16. P. Visscher and L. Falicov. Phys. Rev. B.2, 1518 (1970).
17. J. Vanderkooy and W.R. Datars. Phys. Rev. 156, 671 (1967).